Hepatic Glucagon Receptor Signaling Enhances Insulin-Stimulated Glucose Disposal in Rodents

Teayoun Kim,[1] Cassie L. Holleman,[1] Shelly Nason,[1] Deanna M. Arble,[2] Nickki Ottaway,[3] Joseph Chabenne,[4] Christine Loyd,[1] Jeong-a Kim,[1] Darleen Sandoval,[5] Daniel J. Drucker,[6] Richard DiMarchi,[4,7] Diego Perez-Tilve,[3] and Kirk M. Habegger[1]

Diabetes 2018;67:2157–2166 | https://doi.org/10.2337/db18-0068

Glucagon receptor (GCGR) agonists cause hyperglycemia but also weight loss. However, GCG-like peptide 1 receptor (GLP1R)/GCGR mixed agonists do not exhibit the diabetogenic effects often attributed to GCGR activity. Thus, we sought to investigate the effect of glucagon agonism on insulin action and glucose homeostasis. Acute GCGR agonism induced immediate hyperglycemia, followed by improved glucose tolerance and enhanced glucose-stimulated insulin secretion. Moreover, acute GCGR agonism improved insulin tolerance in a dose-dependent manner in both lean and obese mice. Improved insulin tolerance was independent of GLP1R, FGF21, and hepatic glycogenolysis. Moreover, we observed increased glucose infusion rate, disposal, uptake, and suppressed endogenous glucose production during euglycemic clamps. Mice treated with insulin and GCGR agonist had enhanced phosphorylation of hepatic AKT at Ser^{473}; this effect was reproduced in isolated mouse primary hepatocytes and resulted in increased AKT kinase activity. These data reveal that GCGR agonism enhances glucose tolerance, in part, by augmenting insulin action, with implications for the use of GCGR agonism in therapeutic strategies for diabetes.

Glucagon (GCG) is a 29–amino acid peptide released from α-cells of the pancreatic islet. Its role as a primary counterregulatory hormone to insulin action has long received scientific attention, yet its broader therapeutic potential is underappreciated (1,2). Intriguingly, the antidiabetic actions of GCG-like peptide 1 receptor (GLP1R) agonism are enhanced by the catabolic and hypolipidemic properties of GCG receptor (GCGR) agonism (3–5). Importantly, GLP1R/GCGR mixed agonists do not exhibit the hyperglycemia and glucose intolerance often attributed to GCGR activity, findings that were confirmed in human subjects (6). Moreover, postprandial elevations of GCG and GLP-1 may contribute to improved postprandial glucose homeostasis in Roux-en-Y gastric bypass patients (7,8). How GCGR monoagonism promotes transient glucose intolerance, yet simultaneously contributes to the antidiabetic actions of incretin-based therapies is still unknown. As a counterregulatory hormone with a role in maintaining fasting blood glucose, it is tempting to assume that GCG opposes all actions of insulin. However, the increased concentrations and action of GCG in the fasting state are well suited to potentiate subsequent, insulin-mediated glucose control. In the context of normal physiology, exercise induces GCG secretion (9) and modulates the cephalic response of meal assimilation (10). Altogether these data suggest that GCG may in fact contribute to these states of heightened insulin sensitivity.

Chronic GCGR agonism in diet-induced obese (DIO) mice stimulates weight loss, hyperglycemia, and glucose intolerance (11). Unexpectedly, GCGR signaling in *db/db* mice improved the rate of insulin-stimulated glucose disappearance (k_g) (11). Here we demonstrate that, in

[1]Comprehensive Diabetes Center and Division of Endocrinology, Diabetes, and Metabolism, Department of Medicine, University of Alabama at Birmingham, Birmingham, AL
[2]Department of Biological Sciences, Marquette University, Milwaukee, WI
[3]Metabolic Diseases Institute and Division of Endocrinology, Diabetes, and Metabolism, Department of Medicine, University of Cincinnati, Cincinnati, OH
[4]Novo Nordisk Research Center, Indianapolis, IN
[5]Department of Surgery, University of Michigan, Ann Arbor, MI
[6]Lunenfeld-Tanenbaum Research Institute, Mt. Sinai Hospital, Department of Medicine, University of Toronto, Toronto, Ontario, Canada
[7]Department of Chemistry, Indiana University, Bloomington, IN

Corresponding author: Kirk M. Habegger, kirkhabegger@uabmc.edu, or Diego Perez-Tilve, pereztdo@ucmail.uc.edu.

Received 16 January 2018 and accepted 10 August 2018.

This article contains Supplementary Data online at http://diabetes.diabetesjournals.org/lookup/suppl/doi:10.2337/db18-0068/-/DC1.

addition to its counterregulatory role, hepatic GCGR agonism enhances systemic insulin-stimulated glucose disposal. Together, these data mechanistically elucidate how glucose control may be improved by therapies characterized by GCG agonism.

RESEARCH DESIGN AND METHODS

Animal Models

All studies were approved by and performed according to the guidelines of the Institutional Animal Care and Use Committee of the University of Alabama at Birmingham or the University of Cincinnati. Mice were single or group housed on a 12:12-h light-dark cycle (light on from 0600 h to 1800 h) at 22°C and constant humidity with free access to food and water, except as noted. *Fgf21*-deficient, *Gcgr*-floxed, and *Glp1r*-deficient mice were generated as previously described (12–15), and *Alb*-Cre mice were obtained from The Jackson Laboratory (Bar Harbor, ME). All mice were maintained in our facilities on a C57Bl/6J background and fed a standard chow (5.6% fat, Teklad LM-485) or high-fat diet (58.0 kcal% fat, D12331; Research Diets, New Brunswick, NJ).

Peptides and Inhibitors

Novel GCGR agonists (IUB288 and ASP28, GLU29-GCG) were synthesized as previously described (11,16). Native GCG and insulin (Humulin R) were obtained from American Peptide Co. and Eli Lilly and Co., respectively. Glycogen phosphorylase a/b inhibitor (BAY R3401) was obtained from Sigma-Aldrich and diluted in 0.5% methyl cellulose.

Glucose and Insulin Tolerance Tests

Glucose and insulin tolerance tests (GTTs and ITTs) were performed in 6 h–fasted 8- to 10-week-old chow-fed or 24-week-old DIO male C57Bl/6J mice by i.p. injection of IUB288 (10 nmol/kg) or GCG (10 nmol/kg) 60 min prior to i.p. injection of glucose (2 g/kg, 20% weight for volume [w/v] D-glucose [Sigma-Aldrich] in 0.9% w/v saline) or insulin (0.25–1.0 units/kg in 0.9% w/v saline). ITTs were conducted in lean chow-fed male $Glp1r^{-/-}$ and $Fgf21^{\Delta liver}$ mice at 10–14 weeks old. GTTs and ITTs were conducted in 8- to 12- and 10- to 14-week-old $Gcgr^{\Delta liver}$ mice, respectively. Blood glucose was determined by the TheraSense Freestyle Glucometer. Glucose disappearance rate (k_g) was defined as (Δ blood glucose/min). Insulin and C-peptide were measured from blood collected 60 min after IUB288 challenge.

Intravenous Glucose-Stimulated Insulin Secretion and GCGR Agonist Infusion Tests

Catheters were surgically implanted as previously described (17). Four days after surgery, lean chow-fed 14-week-old male C57Bl/6J mice were fasted for 5 h. IUB288 injection (10 nmol/kg i.p.) was administered 60 min prior to glucose bolus (1 g/kg) delivered via venous catheter. Plasma samples were collected immediately before and 2, 5, 10, and 15 min after infusion. For GCGR agonist infusion studies, chow-fed 14-week-old male C57Bl/6J mice were fasted for 4 h before 120 min ASP28, GLU29-GCG infusion (0.00064 and 0.0064 nmol/min). Mice were administered 0.25 units/kg insulin i.p. and euthanized 20 min later.

Euglycemic Clamps

Clamps were conducted as previously described (17). In brief, catheters were implanted in male 8-week-old chow-fed C57Bl/6J mice. Four to six days postoperative, mice were fasted for 5 h with saline or IUB288 (10 nmol/kg) injected (s.c.) during the final 60 min. Insulin (4 mU/kg/min, diluted in saline) was infused through the venous catheter, and euglycemia (140 mg/dL) was maintained by adjusting the infusion rate of a 20% glucose solution. A tracer equilibration period (t = −120 to 0 min) was used as follows: a 5 μCi bolus of [3-^{3}H]-glucose (PerkinElmer, Boston, MA) was given at t = −120 min followed by a 0.05 μCi/min infusion for 2 h. Somatostatin (SST; EMD Millipore, Temecula, CA), mixed with the [3-^{3}H]-glucose, was infused at 1.5 μg/kg/min from t = −120 to 0 min and at 3 μg/kg/min from t = 0 min to 120 min. At t = 0, [3-^{3}H]-glucose infusion was increased to 0.1 μCi/min to minimize changes in specific activity (SA). The variation of SA was <10% from mean during the last 40 min of clamp, and the slope of SA over time was not significantly different from t = 0. Blood samples (100 μL) were taken at −120, −60, −30, −5, 90, 100, 110, and 120 min for the assessment of glucose, insulin, and glucose SA in plasma. Red blood cells from these samples were recovered by centrifugation and injected via arterial catheter to prevent a hematocrit deficit. A 10 μCi [1-^{14}C]-2 deoxy-D-glucose ([1-^{14}C]-2DG) (MP Biomedicals, Santa Ana, CA) bolus was injected at t = 75 min via carotid arterial catheter to assess glucose uptake. After the clamp, mice were euthanized and tissues (gastrocnemius, soleus, extensor digitorum longus [EDL], quadriceps, liver, gonadal white adipose tissue [WAT], and interscapular brown adipose tissue [BAT]) were snap frozen in liquid nitrogen.

Biochemical Assays

Plasma [3-^{3}H]-glucose, [1-^{14}C]-2DG, and ^3H_2O were measured to determine rate of endogenous glucose production (R_a), rate of glucose disposal (R_d), and uptake as previously described (17). Clamp plasma glucose was measured from 20 μL of deproteinized samples (Glucose Assay Kit; Cell Biolabs, San Diego, CA). Tissue-specific [1-^{14}C]-2DG-6-phosphate ([1-^{14}C]-2DGp) content was determined via perchloric acid–extracted supernatant with Somogyi procedure (18). Glycogen was assessed from [3-^{3}H]-glucose incorporated into ethanol-precipitated glycogen in KOH-digested tissues (19). Plasma glucose SA was calculated from the ratio of plasma glucose radioactivity (dpm) over plasma glucose, multiplied by the ratio of chemical standard evaporated (CSE) to chemical recovery standard (CRS). The [3-^{3}H]-glucose infusion rate (dpm/kg/min) was then calculated from CSE. R_d (mg/kg/min) was determined as the ratio

of the [3-^{3}H]-glucose infusion rate and the plasma glucose SA of (dpm/mg) at the end of the basal period and during the final 30 min of the clamps. Hepatic glucose production rates (Endo R_a; mg/kg/min) were determined by subtracting the steady-state glucose infusion rate (GIR) from R_d. Plasma [^{14}C]-2DG SA (dpm/mg) was obtained by multiplying the radioactivity disappearance area under the curve (AUC) of [^{14}C] in plasma samples by CSE/CRS and then dividing by the average blood glucose during the clamped time course. Finally, tissue-specific 2DG uptake (R_g; μg glucose/mg tissue/min) was determined as the ratio of the [^{14}C]-2DGp in tissue per tissue weight to plasma [^{14}C]-2DG SA. Plasma insulin and C-peptide were measured using mouse ELISA kits (Crystal Chem, Downers Grove, IL).

Primary Hepatocyte Isolation

Primary hepatocytes were prepared from anesthetized lean chow-fed male C57Bl/6J mice as previously described (20). In brief, perfusion buffer (Krebs Ringer with glucose and 0.1 mmol/L EGTA), followed by digestion buffer (Krebs Ringer with glucose, 1.4 mmol/L $CaCl_2$, 50 μg/mL liberase [05401119001; Roche]), was infused into the vena cava via peristaltic pump. Hepatocytes were recovered by centrifugation (50*g* 3 min, three times) and seeded on rat tail type 1 collagen–coated plates in DMEM (10% FBS, 1% penicillin/streptomycin) with all experiments conducted <24 h post-isolation. Hepatocytes were serum starved 60 min prior to 2.5 min insulin or GCG treatment for signaling studies. For glycogen assay, hepatocytes were fasted overnight in serum-free minimum essential medium alpha (1 g/L glucose) prior to 2-h insulin or IUB288 treatment with [3-^{3}H]-glucose.

Immunoblot Analyses

Cell extracts were prepared in lysis buffer (20 mm Tris [pH 6.8], 3.8 mm dithiothreitol, 10% glycerol, 1% SDS, 0.3 mol/L phenylmethylsulfonyl fluoride, and HALT protease inhibitor cocktail [Thermo Fisher Scientific]), rotated for 15 min at 4°C, and centrifuged for 10 min at 4°C. Equivalent protein amounts were separated by 7.5% SDS-PAGE. Resolved fractions were transferred to polyvinylidene fluoride (Bio-Rad Laboratories, Hercules, CA), and phosphorylation was detected using phosphospecific antibodies to AKT^{473}, AKT^{308}, p44/42 MAPK$^{202/204}$, forkhead box protein O1^{24} (FOXO1^{24}), glycogen synthase kinase (GSK) 3α/β$^{21/9}$ (Cell Signaling Technology, Danvers, MA), and IRS1^{612} (LifeTechnologies, Frederick, MD). Phosphorylation was normalized by TGX stain-free technology and by immunoblot analysis with anti-AKT, anti-IRS1, FOXO1, and anti-GSK3 (Cell Signaling Technology). Immunoblots were labeled with goat anti-rabbit horseradish peroxidase–conjugated secondary antibodies, and protein bands were detected and quantified using Clarity ECL, ChemDoc imaging system, and Image Lab 5.0 software (Bio-Rad Laboratories).

AKT Kinase Activity Analysis

Kinase analysis was performed in freshly isolated primary hepatocytes after 2.5 min of insulin/GCG treatments using AKT Kinase Assay Kit (9840; Cell Signaling Technology). Blots from subsequent immunoblot analysis were imaged using LumoGLO substrate provided in kit and normalized to total protein by TGX stain-free technology.

Statistics

All data are represented as mean and SEM. Statistical significance was determined using unpaired Student *t* tests or, where appropriate, one- and two-way ANOVA with multiple comparisons Tukey and Sidak posttest, respectively. Statistics were completed using GraphPad Prism version 6.0 for Macintosh (GraphPad Software, San Diego, CA) and significance assigned when $P < 0.05$.

RESULTS

Acute GCGR Agonism Enhances Insulin Action and Secretion in Mice

To interrogate GCGR agonism in glucose metabolism, we administered the GCGR agonist IUB288 (11,15) to lean chow-fed C57Bl/6J mice via i.p. injection (10 nmol/kg). IUB288 administration resulted in a rapid rise in glycemia and a subtle increase in plasma insulin (Fig. 1*A* and *B*), both returning to baseline levels within 60 min. Surprisingly, an i.p. GTT performed 60 min after single injection of IUB288 in lean mice revealed a significant enhancement of glucose tolerance compared with vehicle (Fig. 1*C*). Importantly, this effect was recapitulated by native GCG (Supplementary Fig. 1*A* and inset). Consistent with prior observations of GCGR-enhanced glucose-stimulated insulin secretion (GSIS) (21), IUB288 pretreatment (−60 min) increased glucose-stimulated insulin levels in response to an i.v. glucose challenge (1 g/kg) (Fig. 1*D* and inset). These data and previous findings (21) suggest that GCG-stimulated enhancements in GSIS likely contribute to the improved glucose tolerance after GCGR agonism.

Acute GCGR Agonism Enhances Insulin Sensitivity in Mice

Although GCGR-dependent potentiation of GSIS may contribute to enhanced glucose tolerance, this mechanism is unlikely to account for any enhancement of insulin action. To assess the effects of GCGR agonism on insulin-dependent glucose disposal, we treated lean mice with IUB288 60 min prior to an ITT (0.5 units/kg). IUB288 significantly enhanced the response to insulin, as determined by both the nadir glucose and the calculated k_g over the initial 30-min period (Fig. 1*E*). To assay endogenous insulin during this test, we measured circulating C-peptide (Fig. 1*F*) and observed that the enhanced insulin action was independent of increased insulin secretion. Importantly, this sensitizing effect was recapitulated by native GCG during both 0.25 units/kg and 0.5 units/kg ITTs without an increase in circulating C-peptide (Supplementary Fig. 1*B–D*) and was similarly observed during coadministration of IUB288 and insulin (Supplementary Fig. 1*E*).

To assess how long improved insulin action remained evident after GCGR agonism, we increased the pretreatment

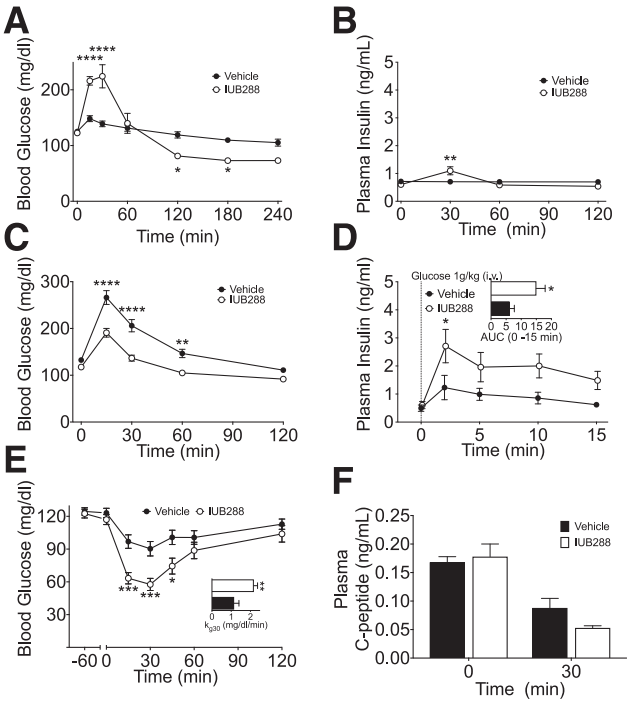

Figure 1—GCGR agonism enhances glucose tolerance and insulin secretion. Blood glucose excursion (*A*) and plasma insulin (*B*) after single i.p. challenge of IUB288 in lean chow-fed C57Bl/6J mice; n = 7–8 mice/group. Blood glucose (*C*) during i.p. GTT with acute IUB288 pretreatment in lean mice (n = 27). Plasma insulin (*D*) and AUC (*D*, inset) during i.v. GSIS with IUB288 pretreatment (n = 7−9). Blood glucose excursion (*E*) and k_g 30 (*E*, inset) during i.p. ITT (0.5 units/kg) with IUB288 pretreatment (s.c. 10 nmol/kg) at −60 min (n = 17–27). Plasma C-peptide (*F*) at time 0 and 30 min during 0.5 units/kg i.p. ITT (n = 10). See also Supplementary Fig. 1. All data are represented as mean ± SEM. $^*P < 0.05$, $^{**}P < 0.01$, $^{***}P < 0.001$, and $^{****}P < 0.0001$, vs. vehicle control mice.

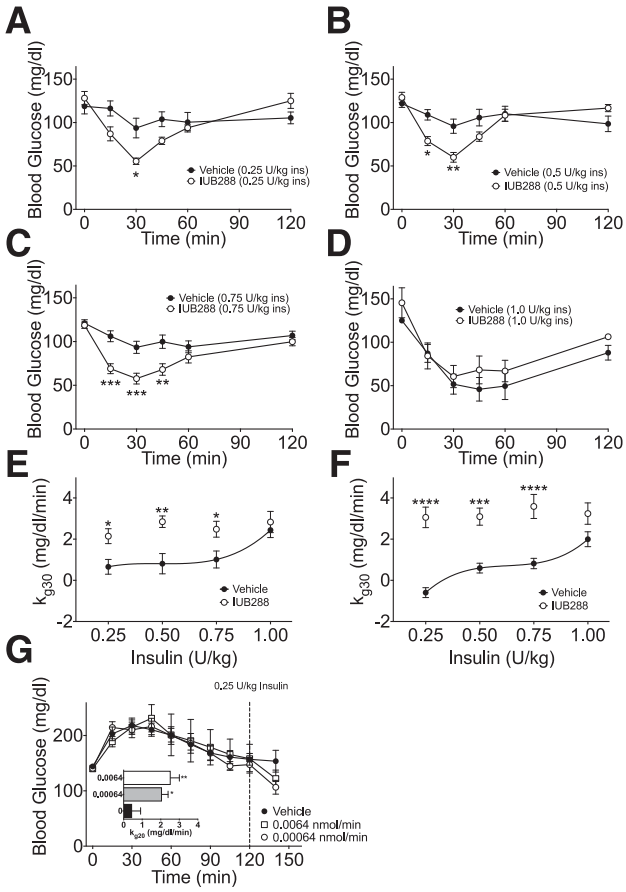

Figure 2—GCGR agonism enhances insulin action across a range of insulin doses. Blood glucose excursion during i.p. ITT at 0.25 (*A*), 0.50 (*B*), 0.75 (*C*), and 1.0 units/kg insulin (*D*) in lean chow-fed mice with simultaneous cotreatment with IUB288 (10 nmol/kg). Rate of glucose change (k_g 30) (*E*) calculated from data in panels *A*–*D*. Rate of glucose change (k_g 30) (*F*) of DIO mice (data from Supplementary Fig. 2). Blood glucose excursion (*G*) and k_g 20 (*G*, inset) after 120 min of continuous ASP28, GLU29-GCG treatment via jugular infusion (n = 7–9). See also Supplementary Figs. 1 and 2. All data are represented as mean ± SEM. n = 8 mice/group. $^*P < 0.05$; $^{**}P < 0.01$; $^{***}P < 0.001$; $^{****}P < 0.0001$.

period (i.e., from 60 to 180 min). Even after this extended pretreatment, we observed a beneficial and dose-dependent effect of IUB288 on insulin action during the ITT (Supplementary Fig. 1*F* and *G*). We next assessed insulin sensitivity after GCGR agonism using ITTs across a range of insulin doses (0.25–1 units/kg). These studies revealed a clear enhancement in insulin action at multiple insulin doses (Fig. 2*A*–*D*), resulting in increased k_g 30 in both lean (Fig. 2*E*) and DIO mice compared with the vehicle controls (Fig. 2*F* and Supplementary Fig. 2*A*–*D*). Similarly, continuous infusion of the short-acting GCGR agonist ASP28, GLU29-GCG 120 min prior to administration of a subthreshold i.p. insulin bolus (0.25 units/kg) increased k_g 20 after GCGR stimulation (Fig. 2*G* and inset). Importantly, this insulin-sensitizing effect occurred in the absence of prior hyperglycemia (Fig. 2*G*), demonstrating independence from GCG-induced hyperglycemia.

Glucagon can activate both stimulatory and inhibitory G-protein pathways via GLP1R (22). To investigate potential GLP1R cross-activation, we conducted an i.p. ITT with IUB288 pretreatment in GLP1R-deficient ($Glp1r^{-/-}$) mice. We found similar insulin-dependent glucose lowering after IUB288 injection in $Glp1r^{-/-}$ mice when compared with their wild-type (WT) littermates (Supplementary Fig. 3*A* and *B*). Likewise, we have reported that GCGR agonism induces the expression and secretion of FGF21, a known insulin sensitizer (11). However, IUB288 improved insulin sensitivity in global (data not shown) and liver-specific, FGF21-deficient ($Fgf21^{\Delta liver}$) mice to a similar extent as observed in control mice (Supplementary Fig. 3*C* and *D*). Together these data suggest that acute GCGR agonism enhanced insulin sensitivity independent of GLP1R signaling or FGF21.

To gain insights into factors contributing to this enhancement of the insulin-dependent glucose metabolism, we performed euglycemic clamps. We conducted these clamps (Fig. 3*A*–*E*) with continuous SST infusion (1.5 μg/kg/min during the preinsulin basal condition and 3 μg/kg/min during insulin infusion, which was maintained through the

termination of the clamp) to control for increased insulin levels observed in IUB288-treated mice (Fig. 1). We also included D-[3-^{3}H]-glucose to interrogate hepatic glucose metabolism and [^{14}C]-2DG to assess tissue-specific glucose uptake. Mice receiving IUB288 initially displayed hyperglycemia (Fig. 3*A*) that was resolved by the second hour of insulin infusion. However, under clamp conditions (t = 90–120), we observed a striking increase in GIR in IUB288-treated mice (Fig. 3*B*). Importantly, we observed similar GIR potentiation in euglycemic clamp studies conducted without SST (data not shown). Plasma insulin measured at baseline (t = 0) and 120 min in our SST-based euglycemic clamp revealed a slight elevation (P = 0.0025, two-way ANOVA) (Fig. 3*C*). Importantly, the enhanced GIR observed in IUB288-treated mice was not attributable to differential levels of circulating insulin (Fig. 3*C*). R_d was likewise increased over vehicle treatment (Fig. 3*D*). Altogether, these data demonstrate that GCGR agonism enhances whole-body insulin sensitivity.

R_a in IUB288-treated mice was reduced to a greater extent as compared with vehicle controls ($P < 0.0001$ in steady state) (Fig. 3*E* and inset), suggesting hepatic insulin sensitivity was enhanced despite the fact that baseline R_a was predictably elevated by IUB288 ($P < 0.01$). GCGR agonism significantly reduced liver glycogen content during euglycemic clamp ($P < 0.01$) (Fig. 4*A*). Likewise, insulin failed to revert the reduction in glycogen promoted by IUB288 in isolated primary hepatocytes (Fig. 4*B*). Hepatocyte glycogen depletion enhances glycogen synthesis and glucose uptake (23) and also stimulates adipocyte lipolysis via a hepatic–central nervous system–adipose signaling axis (24). To test if depletion of hepatic glycogen stores also acts as a precipitating signal to enhance whole-body insulin sensitivity, we blocked glycogenolysis via the glycogen phosphorylase a/b inhibitor BAY R3401 (25). BAY R3401 was administered 60 min prior to IUB288 treatment (i.e., t = −120) and was sufficient to block 70% of the acute GCGR agonist–stimulated hyperglycemia and to reduce glycemia in lean chow-fed mice (Supplementary Fig. 4*A* and *B*). BAY R3401 pretreatment likewise improved glucose tolerance (Supplementary Fig. 4*C*), yet did not reduce the incremental AUC, in these mice (Supplementary Fig. 4*D*, bars 1 and 3). As in our prior studies, IUB288 pretreatment induced transient hyperglycemia, yet improved glucose tolerance (excursion and incremental AUC), in vehicle-pretreated mice (Supplementary Fig. 4*C* and *D*). However, inhibition of glycogenolysis failed to reduce GCG-stimulated enhancement of glucose tolerance (Supplementary Fig. 4*D*, bars 2 and 4). Altogether, these data suggest that GCGR signaling cooperates with insulin to reduce glucose output independent of its effects on glycogen metabolism.

Unlike in liver, skeletal muscle glycogen was unchanged by IUB288 (Fig. 4*A*). However, we observed elevated [^{14}C]-2DG uptake into EDL, quadriceps, gastrocnemius, and soleus (Fig. 4*C*). In contrast to skeletal muscle, glucose uptake was unchanged in WAT (Fig. 4*C*), yet BAT appears to be the primary site of IUB288-stimulated glucose disposal, as [^{14}C]-2DG accumulation was increased by fivefold compared with saline ($P < 0.005$) (Fig. 4*D*).

Interaction of Hepatic Glucagon and Insulin Receptor Signaling

Considering high-level expression of both GCGR and insulin receptor (INSR) in liver, we reasoned that hepatic

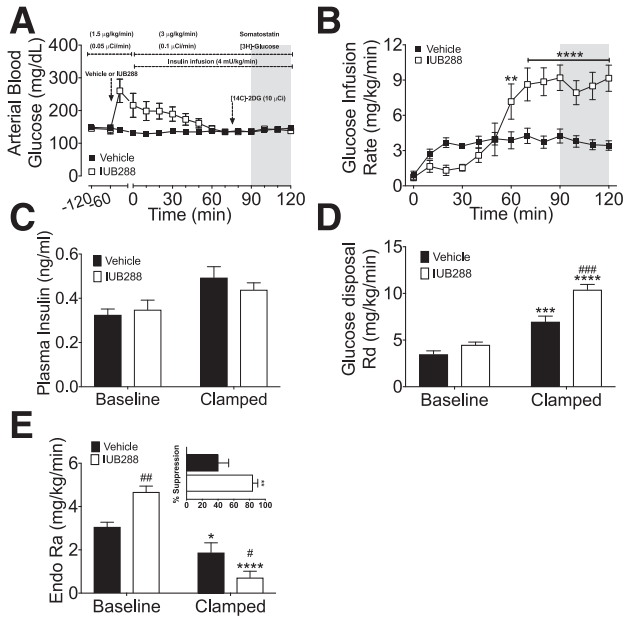

Figure 3—GCGR agonism enhances hepatic insulin sensitivity during euglycemic clamp. Blood glucose (*A*) and GIR (*B*) during labeled euglycemic clamp. Plasma insulin (*C*), R_d (*D*), R_a (*E*), and suppression of R_a (*E*, inset) during labeled euglycemic clamp. All data are represented as mean ± SEM (n = 6–7 mice). See also Supplementary Fig. 5. *$P < 0.05$, **$P < 0.01$, ***$P < 0.001$, and ****$P < 0.0001$, vs. baseline time point; #$P < 0.05$, ##$P < 0.01$, and ###$P < 0.001$, vs. vehicle within time points.

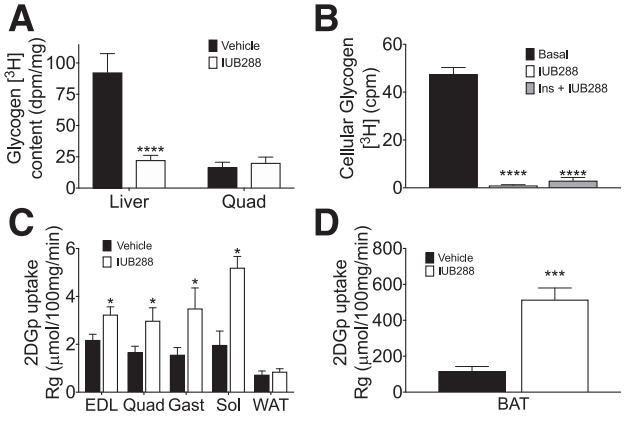

Figure 4—GCGR agonism enhances insulin-stimulated nonhepatic glucose uptake during euglycemic clamp. Liver and quadriceps glycogen content (*A*) after labeled euglycemic clamp. Cellular glycogen levels (*B*) after 2-h IUB288 or IUB288 and insulin cotreatment in primary hepatocytes (n = 3–4 observations). [^{14}C]-2DG uptake into EDL, quadriceps, gastrocnemius, soleus, and epididymal WAT (*C*) and BAT (*D*). All data are represented as mean ± SEM (n = 6–7 mice). See also Supplementary Fig. 5. *$P < 0.05$; ***$P < 0.001$; ****$P < 0.0001$.

interaction between GCGR and INSR signaling pathways contributed to enhanced insulin sensitivity. We injected chow-fed mice with IUB288 or vehicle 60 min prior to an i.p. bolus of insulin or vehicle. Ten minutes later, components of the insulin signaling pathway were analyzed in liver tissue. IUB288 pretreatment increased the insulin-stimulated phosphorylation at AKT^{Ser473}, but not AKT^{Thr308} (Fig. 5*A–C*), suggesting that GCGR-stimulated enhancement of insulin sensitivity may rely upon a site-specific potentiation of AKT phosphorylation. We next treated isolated hepatocytes with GCG over a range of insulin concentrations to assess cell-autonomous interactions between GCGR and INSR signaling. Phosphorylation of IRS1^{Tyr612} and AKT^{Thr308} by insulin was unaffected by the GCG cotreatment (Fig. 5*D* and *F* and Supplementary Fig. 5*A* and *B*). Consistent with our in vivo studies, GCG cotreatment directly enhanced insulin-stimulated AKT^{Ser473} phosphorylation (Fig. 5*E*). We also observed enhanced phosphorylation of the AKT target, GSK3α/β ($P < 0.01$) (Supplementary Fig. 5*A–D*), but not FOXO1 (Supplementary Fig. 5*A* and *B*).

To directly test for enhanced AKT activity, we measured kinase activity of isolated AKT in vitro. Phosphorylated AKT was immunoprecipitated from primary hepatocyte cell lysates prior to incubation with a target peptide. Similar to our observations in liver tissue and isolated hepatocytes, insulin-stimulated AKT activity was significantly enhanced by cotreatment with GCG (Fig. 5*G* and *H*).

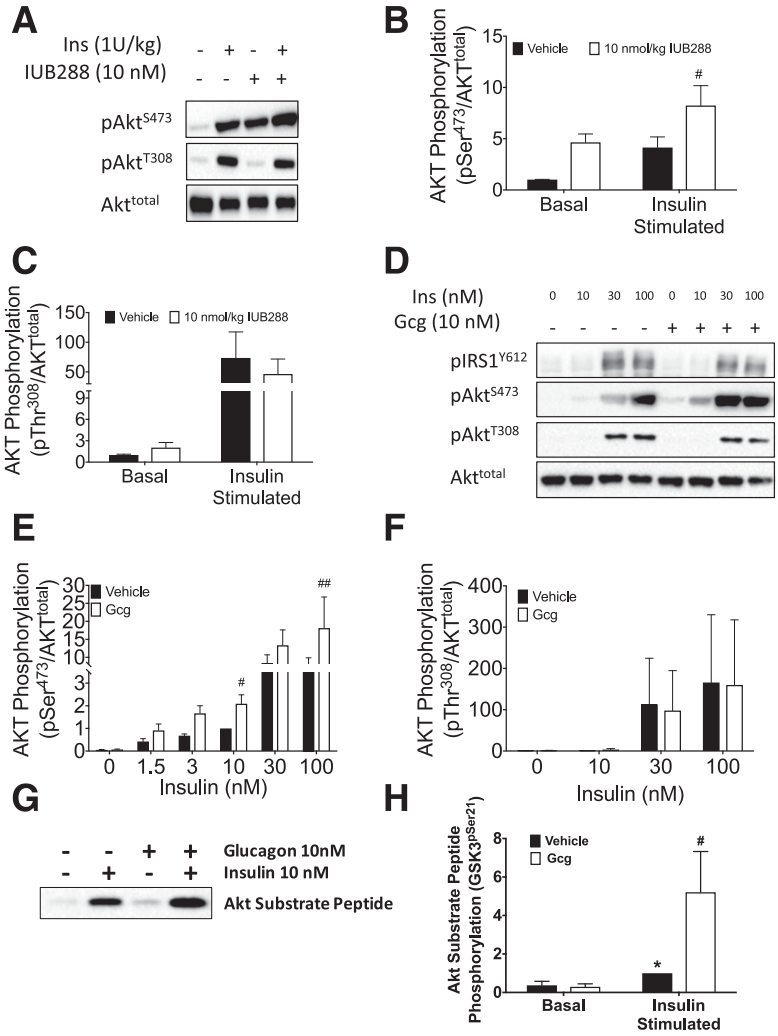

Figure 5—Convergence of GCGR and insulin signaling at AKT. Immunoblot analysis of liver AKT phosphorylation in response to insulin and IUB288. IUB288 (10 nmol/kg) injected 60 min prior to 10-min insulin challenge. Representative images of phosphorylation on residues Ser^{473} and Thr^{308} (*A*) and densitometric quantification (*B* and *C*) of seven to eight mice per group. Immunoblot analysis of hepatocyte insulin signaling in response to insulin and GCG cotreatment (*D–F*). Representative images (*D*) and densitometric quantification (*E* and *F*) of six independent observations. Kinase activity analysis of hepatocyte AKT in response to insulin and IUB288 cotreatment. Representative image of in vitro phosphorylation of exogenous AKT substrate (GSK3) (*G*). Densitometric quantification (*H*) of four independent observations. See also Supplementary Fig. 6. All data are represented as mean ± SEM. *$P < 0.05$, vs. baseline time point; #$P < 0.05$ and ##$P < 0.01$, vs. vehicle within time points.

Together these data suggest that GCGR-dependent enhancement of insulin sensitivity is mediated via increased AKT activity.

Analysis of liver samples from clamped mice identified a similar increase in liver AKT^{Ser473} phosphorylation (Supplementary Fig. 6*A* and *E*) with reduced phosphorylation at $IRS1^{Tyr612}$, AKT^{Thr308}, and p44/42 $MAPK^{Thr202/Tyr204}$ (Supplementary Fig. 6*B–E*). Although glucose uptake was enhanced in EDL, AKT^{Ser473} phosphorylation was reduced in this tissue, whereas AKT^{Thr308} phosphorylation was elevated and phosphorylation at $IRS1^{Tyr612}$ and p44/42 $MAPK^{Thr202/Tyr204}$ was unchanged (Supplementary Fig. 6*A–D* and *F*). Finally, in BAT, where glucose uptake was most positively regulated, phosphorylation at AKT^{Ser473}, AKT^{Thr308}, and p44/42 $MAPK^{Thr202/Tyr204}$ were all enhanced, with a similar trend at $IRS1^{Tyr612}$ (Supplementary Fig. 6*A–D* and *G*). Together these data further support a direct and indirect contribution of multiple tissues to the GCGR-dependent enhancement of glucose clearance.

Hepatic Glucagon Receptors Contribute to GCGR-Mediated Improvements in Insulin Action

To investigate the physiological contribution of hepatic GCGRs, we used mice deficient for hepatic *Gcgr* ($Gcgr^{\Delta liver}$). As previously described (14,15), these mice exhibit reduced fasting blood glucose (Fig. 6*A*), are refractory to a single provocative IUB288 challenge (Fig. 6*B*), and display dramatically enhanced glucose tolerance (Fig. 6*C*). Unlike in WT mice, IUB288 had little effect on glucose excursion in $Gcgr^{\Delta liver}$ mice (Fig. 6*C* and *D*). To further dissect the contribution of the hepatic GCGR, we challenged mice with an ITT (0.25 units/kg) and observed reduced blood glucose (Fig. 6*E*) and enhanced k_g (Fig. 6*F*) in WT, but not $Gcgr^{\Delta liver}$, mice. Moreover, GCG cotreatment enhanced insulin-stimulated AKT^{Ser473} phosphorylation in isolated primary hepatocytes from WT, but not $Gcgr^{\Delta liver}$, mice (Fig. 6*G* and *H*), suggesting that hepatic GCGR signaling contributes to insulin-dependent improvement in glycemic control.

DISCUSSION

Data presented here elucidate a novel role for GCGR signaling in insulin sensitivity. As a counterregulatory hormone, it is tempting to assume that GCG opposes all of insulin's actions. However, GCG secretion and action in the fasting state make it well-suited to potentiate subsequent insulin action. In normal physiology, these data and the previously described prandial GCG spike (26) suggest that GCG may act as a preparatory component for the postprandial state. Thus, whereas chronic GCGR activation impairs glucose tolerance, acute agonism synergistically enhances insulin action and may also potentiate glucose-dependent insulin secretion.

Mechanistically, we observed that hepatic GCGR-deficient mice were resistant to GCG-mediated potentiation of insulin action, suggesting that the liver is likely the primary site of action. Although these findings highlight the liver (and presumably hepatocytes) as the tissue responsible for this novel GCGR action, a caveat must be acknowledged in this interpretation. Specifically, the $Gcgr^{\Delta liver}$ mouse is characterized by supraphysiological levels of GLP-1 and FGF21 (27), both potent sensitizers of insulin action, which may contribute to the reported improvement in glucose tolerance (27). In the context of this study, these factors may act to mask any subtle differences between the IUB288- and vehicle-pretreated $Gcgr^{\Delta liver}$ mice. Consistent with this observation, we observed a small, but statistically significant, difference in glucose excursion between the IUB288- and vehicle-pretreated $Gcgr^{\Delta liver}$ mice 30 min after glucose challenge. Thus, although the liver is likely the primary site of action, it is possible that the direct potentiation of AKT^{Ser473} phosphorylation and subsequent activity observed in liver may also occur in other tissues.

The acute action of GCGR agonsim to elevate glycemia invokes the possibility that this transient hyperglycemia may trigger insulin secretion and thus improve glucose homeostasis. However, infusion of a short-acting GCGR agonist at doses insufficient to induce hyperglycemia still resulted in a clear and significant increase in insulin action. Likewise, blockade of glycogenolysis (via BAY R3401) (Supplementary Fig. 4) ablated GCGR agonist–induced hyperglycemia, but not IUB288 enhancement of glucose tolerance. Moreover, our euglycemic clamp protocol included continuous SST infusion to eliminate potential endogenous insulin secretion. We observed GCG-enhanced insulin actions, including improved glucose tolerance, suppressed hepatic glucose output, and enhanced glucose uptake in the presence of SST. Together we interpret these data to suggest that insulin secretion, downstream of GCGR agonist–induced hyperglycemia, is not the mechanism underlying this enhanced glucose homeostasis.

Although these data cannot exclude a possible cross-activation of other receptors (i.e., GIPR), these insulin-sensitizing effects are clearly GCGR dependent. Along these lines, hepatic glycogen is known to regulate adipocyte lipolysis via a hepatic–central nervous system–adipose signaling axis (24). This regulatory pathway is of interest in that it is stimulated by depleted hepatic glycogen levels, similar to what we observe after GCGR agonsim. However, pharmacological blockade of glycogenolysis had no effect on GCG-stimulated enhancement of glucose tolerance. We interpret these results to conclude that the effects of GCGR agonsim on glucose tolerance are independent of its effects on glycogen metabolism. Although we hypothesize that GCGR and INSR signaling are interacting in a cell-autonomous manner at the hepatocyte, insulin also suppresses hepatic glucose production via reduction of circulating free fatty acids (28) (i.e., independent of liver INSR or GCGR signaling). Thus, although the liver is likely the primary site of action, it is possible that the direct potentiation of AKT^{Ser473} phosphorylation and subsequent activity observed in liver may also occur in other tissues. Of particular note was the enhanced uptake observed in

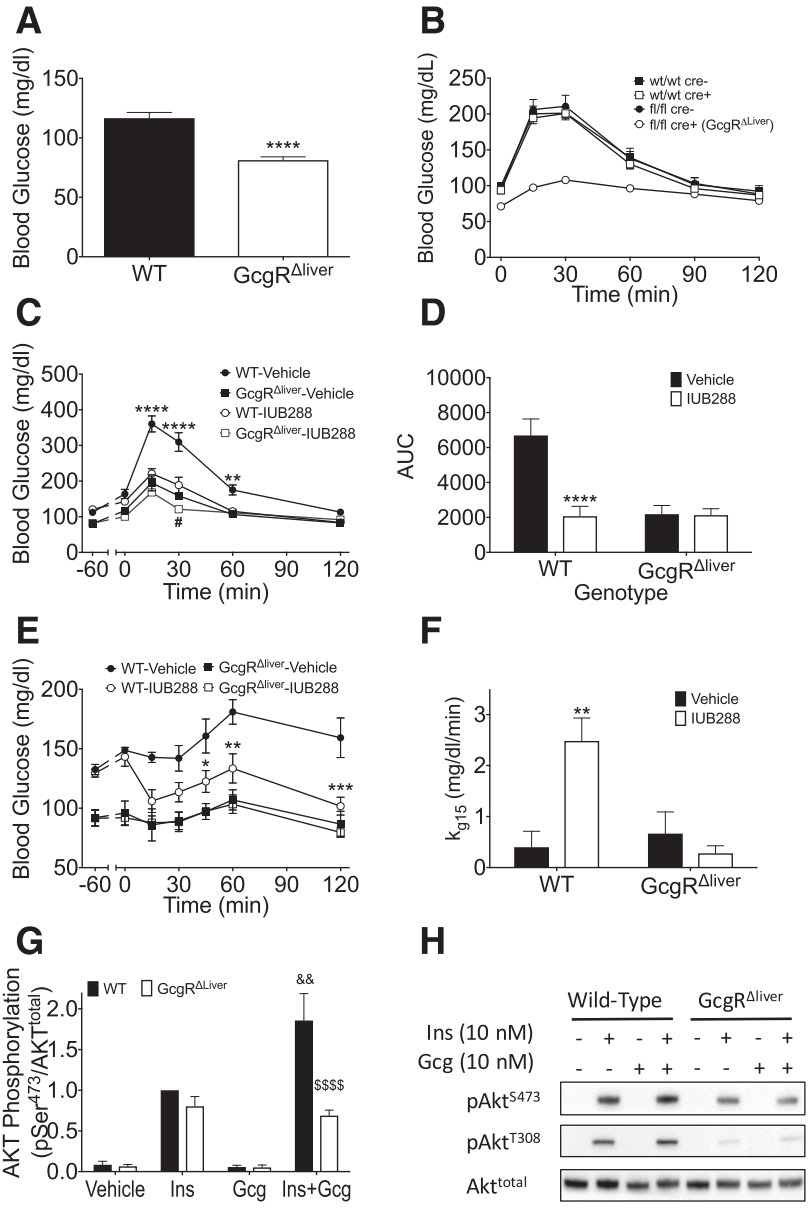

Figure 6—Hepatic receptors contribute to GCGR-mediated improvements in insulin action. Fasting blood glucose (*A*) and i.p. IUB288-stimulated blood glucose excursion (*B*) in WT and *Gcgr*$^{\Delta liver}$ mice. GTT (*C*) and AUC analysis (*D*) in WT and *Gcgr*$^{\Delta liver}$ mice with IUB288 pretreatment. ITT (*E*) and k_g 15 analysis (*F*) in WT and *Gcgr*$^{\Delta liver}$ mice with 60-min IUB288 pretreatment administered s.c. at 10 nmol/kg throughout. Immunoblot analysis of AKT phosphorylation in response to insulin and GCG cotreatment in hepatocytes isolated from WT or *Gcgr*$^{\Delta liver}$ mice (*G* and *H*). All data are represented as mean ± SEM. *$P < 0.05$, **$P < 0.01$, ***$P < 0.001$, and ****$P < 0.0001$, WT vehicle vs. WT IUB288; #$P < 0.05$, *Gcgr*$^{\Delta liver}$ vehicle vs. *Gcgr*$^{\Delta liver}$ IUB288; &&$P < 0.01$, WT insulin vs. WT insulin + IUB288; \$\$\$\$$P < 0.0001$, WT insulin + IUB288 vs. *Gcgr*$^{\Delta liver}$ insulin + IUB288.

skeletal muscle. Given that GCGR is poorly expressed in skeletal muscle (if at all) (29), this effect is likely mediated indirectly via an alternative endocrine signal and not the direct interactions of GCGR and INSR signaling in these cells.

Importantly, during the preparation of this article, Alonge et al. (30) reported the cooperative intersection of GCG and insulin signaling in the transcriptional regulation of *Fgf21* expression. This report, along with our current studies, provides strong evidence for intracellular and cooperative overlap between these two counterregulating hormones. The physiological relevance of Ser^{473} phosphorylation is controversial. However, an emerging view suggests that it precedes Thr^{308} phosphorylation, facilitating activation by PDK1 (31). The mechanistic target of rapamycin complex 2 (mTORC2) is responsible for insulin-stimulated AKT^{Ser473} phosphorylation (32). Thus, potentiation of Ser^{473} phosphorylation suggests that GCGR agonism may augment this pathway. However, other known mTORC2 targets, paxillin, protein kinase Cα (33), and the serum- and glucocorticoid-induced protein kinase (34), remained unaffected

by GCG (data not shown). These data suggest target-specific activation of the complex after GCGR agonism, or inhibition of a phosphatase specifically targeting AKT-Ser^{473}, such as PH domain leucine-rich repeat protein phosphatase (35). Testing these hypotheses will require further experimentation.

The findings described here add to the growing therapeutic attributes of GCGR activation. Specifically, recent reports suggest that coagonists containing GCGR activity produce superior glucose control as compared with GLP-1, GIP, or thyroid hormones alone (3–5,36). Likewise, our data may provide mechanistic insight into the paradoxical improvements in the average level of glycemia and a reduction in hyperglycemic events observed in patients using a wearable, bihormonal (GCG and insulin) bionic pancreas (37). Thus, these data suggest that GCGR agonism acts both at the level of the liver and pancreas to improve postprandial glycemia. Further, they provide mechanistic insight into the "paradoxical" improvement in glucose homeostasis seen in GCGR-targeted therapeutics.

Acknowledgments. The authors acknowledge David D'Alessio (Duke University), Stuart Frank and Anath Shalev (University of Alabama at Birmingham) for helpful discussion, and Jessica Antipenko (University of Alabama at Birmingham), Joyce Sorrel, Sarah Amburgy, Jenna Holland (University of Cincinnati), and Chelsea Penny and Leslie Wilkinson (University of Alabama at Birmingham) for their technical assistance.

Funding. This project was supported by the National Heart, Lung, and Blood Institute (R01-HL-128695 [J.K.]) and the National Institute of Diabetes and Digestive and Kidney Diseases (R01-DK-082480 [D.S.], R01-DK-077975 [D.P.-T.], 5K01-DK-098319 and 1R01-DK-112934 [K.M.H.], and P30-DK-079626). This work was also supported by the Canada Research Chairs Program (D.J.D.), the Canadian Institutes of Health Research (136942 and 154321), and the American Diabetes Association (ADA) (1-13-JF-21 [K.M.H.]).

Duality of Interest. No potential conflicts of interest relevant to this article were reported.

Author Contributions. T.K. conceived and designed the study, generated experimental data, analyzed and interpreted data, and drafted the manuscript. C.L.H., S.N., D.M.A., N.O., J.C., and C.L. generated experimental data. J.K., D.S., D.J.D., R.D., and D.P.-T. advised on the study concept and critically revised the manuscript. K.M.H. conceived and designed the study, analyzed and interpreted data, and drafted the manuscript. K.M.H. is the guarantor of this work and, as such, had full access to all the data in the study and takes responsibility for the integrity of the data and the accuracy of the data analysis.

Prior Presentation. Portions of this work were presented at the 74th Scientific Sessions of the American Diabetes Association, San Francisco, CA, 13–17 June 2014; the 75th Scientific Sessions of the American Diabetes Association, Boston, MA, 5–9 June 2015; and the 76th Scientific Sessions of the American Diabetes Association, New Orleans, LA, 10–14 June 2016.

References

1. Habegger KM, Heppner KM, Geary N, Bartness TJ, DiMarchi R, Tschöp MH. The metabolic actions of glucagon revisited. Nat Rev Endocrinol 2010;6:689–697
2. Müller TD, Finan B, Clemmensen C, DiMarchi RD, Tschöp MH. The new biology and pharmacology of glucagon. Physiol Rev 2017;97:721–766
3. Day JW, Ottaway N, Patterson JT, et al. A new glucagon and GLP-1 co-agonist eliminates obesity in rodents. Nat Chem Biol 2009;5:749–757
4. Clemmensen C, Chabenne J, Finan B, et al. GLP-1/glucagon coagonism restores leptin responsiveness in obese mice chronically maintained on an obesogenic diet. Diabetes 2014;63:1422–1427
5. Finan B, Yang B, Ottaway N, et al. A rationally designed monomeric peptide triagonist corrects obesity and diabetes in rodents. Nat Med 2015;21:27–36
6. Tan TM, Field BC, McCullough KA, et al. Coadministration of glucagon-like peptide-1 during glucagon infusion in humans results in increased energy expenditure and amelioration of hyperglycemia. Diabetes 2013;62:1131–1138
7. Habegger KM, Heppner KM, Amburgy SE, et al. GLP-1R responsiveness predicts individual gastric bypass efficacy on glucose tolerance in rats. Diabetes 2014;63:505–513
8. Campos GM, Rabl C, Havel PJ, et al. Changes in post-prandial glucose and pancreatic hormones, and steady-state insulin and free fatty acids after gastric bypass surgery. Surg Obes Relat Dis 2014;10:1–8
9. Krishna MG, Coker RH, Lacy DB, Zinker BA, Halseth AE, Wasserman DH. Glucagon response to exercise is critical for accelerated hepatic glutamine metabolism and nitrogen disposal. Am J Physiol Endocrinol Metab 2000;279:E638–E645
10. Powley TL. The ventromedial hypothalamic syndrome, satiety, and a cephalic phase hypothesis. Psychol Rev 1977;84:89–126
11. Habegger KM, Stemmer K, Cheng C, et al. Fibroblast growth factor 21 mediates specific glucagon actions. Diabetes 2013;62:1453–1463
12. Hotta Y, Nakamura H, Konishi M, et al. Fibroblast growth factor 21 regulates lipolysis in white adipose tissue but is not required for ketogenesis and triglyceride clearance in liver. Endocrinology 2009;150:4625–4633
13. Scrocchi LA, Brown TJ, MaClusky N, et al. Glucose intolerance but normal satiety in mice with a null mutation in the glucagon-like peptide 1 receptor gene. Nat Med 1996;2:1254–1258
14. Longuet C, Robledo AM, Dean ED, et al. Liver-specific disruption of the murine glucagon receptor produces α-cell hyperplasia: evidence for a circulating α-cell growth factor. Diabetes 2013;62:1196–1205
15. Kim T, Nason S, Holleman C, et al. Glucagon-receptor signaling regulates energy metabolism via hepatic farnesoid X receptor and fibroblast growth factor 21. Diabetes 2018
16. Lockie SH, Heppner KM, Chaudhary N, et al. Direct control of brown adipose tissue thermogenesis by central nervous system glucagon-like peptide-1 receptor signaling. Diabetes 2012;61:2753–2762
17. Kim T, He L, Johnson MS, et al. Carnitine palmitoyltransferase 1b deficiency protects mice from diet-induced insulin resistance. J Diabetes Metab 2014;5:361
18. Mészáros K, Lang CH, Bagby GJ, Spitzer JJ. Contribution of different organs to increased glucose consumption after endotoxin administration. J Biol Chem 1987;262:10965–10970
19. Kim HJ, Higashimori T, Park SY, et al. Differential effects of interleukin-6 and -10 on skeletal muscle and liver insulin action in vivo. Diabetes 2004;53:1060–1067
20. Li WC, Ralphs KL, Tosh D. Isolation and culture of adult mouse hepatocytes. Methods Mol Biol 2010;633:185–196
21. Huypens P, Ling Z, Pipeleers D, Schuit F. Glucagon receptors on human islet cells contribute to glucose competence of insulin release. Diabetologia 2000;43:1012–1019
22. Weston C, Poyner D, Patel V, Dowell S, Ladds G. Investigating G protein signalling bias at the glucagon-like peptide-1 receptor in yeast. Br J Pharmacol 2014;171:3651–3665
23. Winnick JJ, An Z, Kraft G, et al. Liver glycogen loading dampens glycogen synthesis seen in response to either hyperinsulinemia or intraportal glucose infusion. Diabetes 2013;62:96–101
24. Izumida Y, Yahagi N, Takeuchi Y, et al. Glycogen shortage during fasting triggers liver-brain-adipose neurocircuitry to facilitate fat utilization [published correction appears in Nat Commun 2013;4:2930]. Nat Commun 2013;4:2316
25. Bergans N, Stalmans W, Goldmann S, Vanstapel F. Molecular mode of inhibition of glycogenolysis in rat liver by the dihydropyridine derivative, BAY R3401: inhibition and inactivation of glycogen phosphorylase by an activated metabolite. Diabetes 2000;49:1419–1426
26. Geary N. Pancreatic glucagon signals postprandial satiety. Neurosci Biobehav Rev 1990;14:323–338

27. Omar BA, Andersen B, Hald J, Raun K, Nishimura E, Ahrén B. Fibroblast growth factor 21 (FGF21) and glucagon-like peptide 1 contribute to diabetes resistance in glucagon receptor-deficient mice. Diabetes 2014;63:101–110
28. Titchenell PM, Chu Q, Monks BR, Birnbaum MJ. Hepatic insulin signalling is dispensable for suppression of glucose output by insulin in vivo. Nat Commun 2015;6:7078
29. Hansen LH, Abrahamsen N, Nishimura E. Glucagon receptor mRNA distribution in rat tissues. Peptides 1995;16:1163–1166
30. Alonge KM, Meares GP, Hillgartner FB. Glucagon and insulin cooperatively stimulate fibroblast growth factor 21 gene transcription by increasing the expression of activating transcription factor 4. J Biol Chem 2017;292:5239–5252
31. Scheid MP, Marignani PA, Woodgett JR. Multiple phosphoinositide 3-kinase-dependent steps in activation of protein kinase B. Mol Cell Biol 2002;22:6247–6260
32. Sarbassov DD, Guertin DA, Ali SM, Sabatini DM. Phosphorylation and regulation of Akt/PKB by the rictor-mTOR complex. Science 2005;307:1098–1101
33. Sarbassov DD, Ali SM, Kim DH, et al. Rictor, a novel binding partner of mTOR, defines a rapamycin-insensitive and raptor-independent pathway that regulates the cytoskeleton. Curr Biol 2004;14:1296–1302
34. Laplante M, Sabatini DM. mTOR signaling in growth control and disease. Cell 2012;149:274–293
35. Gao T, Furnari F, Newton AC. PHLPP: a phosphatase that directly dephosphorylates Akt, promotes apoptosis, and suppresses tumor growth. Mol Cell 2005;18:13–24
36. Finan B, Clemmensen C, Zhu Z, et al. Chemical hybridization of glucagon and thyroid hormone optimizes therapeutic impact for metabolic disease. Cell 2016;167:843–857.e814
37. Russell SJ, El-Khatib FH, Sinha M, et al. Outpatient glycemic control with a bionic pancreas in type 1 diabetes. N Engl J Med 2014;371:313–325